Lasers in Surgery and Medicine 25:22–37 (1999)

Holmium:YAG Laser Lithotripsy: A Dominant Photothermal Ablative Mechanism With Chemical Decomposition of Urinary Calculi

Kin Foong Chan, MSE,[1]* George J. Vassar, MD,[2] T. Joshua Pfefer, PhD,[3] Joel M. H. Teichman, MD,[2] Randolph D. Glickman, PhD,[4] Susan T. Weintraub, PhD,[5] and Ashley J. Welch, PhD[1,2]

[1]Department of Electrical and Computer Engineering, University of Texas at Austin, Austin, Texas 78712
[2]Division of Urology, University of Texas Health Science Center, San Antonio, Texas 78284
[3]Biomedical Engineering Program, University of Texas at Austin, Austin, Texas 78712
[4]Department of Ophthalmology, University of Texas Health Science Center, San Antonio, Texas 78284
[5]Department of Biochemistry, University of Texas Health Science Center, San Antonio, Texas 78284

Background and Objective: **Evidence is presented that the fragmentation process of long-pulse Holmium:YAG (Ho:YAG) lithotripsy is governed by photothermal decomposition of the calculi rather than photomechanical or photoacoustical mechanisms as is widely thought. The clinical Ho:YAG laser lithotriptor (2.12 μm, 250 μs) operates in the free-running mode, producing pulse durations much longer than the time required for a sound wave to propagate beyond the optical penetration depth of this wavelength in water. Hence, it is unlikely that shock waves are produced during bubble formation. In addition, the vapor bubble induced by this laser is not spherical. Thus the magnitude of the pressure wave produced at cavitation collapse does not contribute significantly to lithotripsy.**
Study Design/Materials and Methods: **A fast-flash photography setup was used to capture the dynamics of urinary calculus fragmentation at various delay times following the onset of the Ho:YAG laser pulse. These images were concurrently correlated with pressure measurements obtained with a piezoelectric polyvinylidene-fluoride needle-hydrophone. Stone mass-loss**

Contract grant sponsor: Office of Naval Research Free Electron Laser Biomedical Science Program; contract grant number: N00014-91-J-1564 (UT Austin); contract grant sponsor: The Albert W. and Clemmie A. Caster Foundation (UT Austin); contract grant sponsor: The Research to Prevent Blindness (UTHSCSA); contract grant sponsor: The Air Force Office of Scientific Research; contract grant number: F49620-98-1-0210 (UTHSCSA); contract grant sponsor: The Air Force Office of Scientific Research through MURI from DDR&E; contract grant number: F49620-98-1-0480 (UT Austin).

*Correspondence to: Kin Foong Chan, Department of Electrical and Computer Engineering, University of Texas at Austin, ENS 610, Austin, TX 78712.
E-mail: kfchan@ccwf.cc.utexas.edu

Accepted 2 February 1999

measurements for ablation of urinary calculi (1) in air (dehydrated and hydrated) and in water, and (2) at pre-cooled and at room temperatures were compared. Chemical and composition analyses were performed on the ablation products of several types of Ho:YAG laser irradiated urinary calculi, including calcium oxalate monohydrate (COM), calcium hydrogen phosphate dihydrate (CHPD), magnesium ammonium phosphate hexahydrate (MAPH), cystine, and uric acid calculi.
Results: **When the optical fiber was placed perpendicularly in contact with the surface of the target, fast-flash photography provided visual evidence that ablation occurred approximately 50 μs after the initiation of the Ho:YAG laser pulse (250–350 μs duration; 375–400 mJ per pulse), long before the collapse of the cavitation bubble. The measured peak acoustical pressure upon cavitation collapse was negligible (< 2 bars), indicating that photomechanical forces were not responsible for the observed fragmentation process. When the fiber was placed in parallel to the calculus surface, the pressure peaks occurring at the collapse of the cavitation were on the order of 20 bars, but no fragmentation occurred. Regardless of fiber orientation, no shock waves were recorded at the beginning of bubble formation. Ablation of COM calculi (a total of 150 J; 0.5 J per pulse at an 8-Hz repetition rate) revealed different Ho:YAG efficiencies for dehydrated calculus, hydrated calculus, and submerged calculus. COM and cystine calculi, pre-cooled at –80°C and then placed in water, yielded lower mass-loss during ablation (20 J, 1.0 J per pulse) compared to the mass-loss of calculi at room temperature. Chemical analyses of the ablated calculi revealed products resulting from thermal decomposition. Calcium carbonate was found in samples composed of COM calculi; calcium pyrophosphate was found in CHPD samples; free sulfur and cysteine were discovered in samples composed of cystine samples; and cyanide was found in samples of uric acid calculi.**
Conclusion: **These experimental results provide convincing evidence that long-pulse Ho:YAG laser lithotripsy causes chemical decomposition of urinary calculi as a consequence of a dominant photothermal mechanism. Lasers Surg. Med. 25:22–37, 1999.** **© 1999 Wiley-Liss, Inc.**

Key words: fast-flash photography; kidney stones; laser lithotripsy; long-pulse Ho:YAG; mass-loss; photoacoustical pressure waves; photothermal mechanism; thermal breakdown

INTRODUCTION

Long-pulse Holmium:YAG (Ho:YAG) laser (2.12 μm) has been used extensively in urology for laser lithotripsy [1–12]. The Ho:YAG laser is an attractive alternative to other conventional laser lithotriptors such as the Q-switched Nd:YAG, pulsed-dye and ruby lasers because it offers high power (~ kW, up to several Joules at 250-μs duration) pulses that are transmittable via a low OH^- optical fiber. As a solid state laser, it is less expensive and easier to maintain than pulsed-dye systems. Whereas it has been reported that the Q-switched Nd:YAG laser is not efficient in fragmenting calcium oxalate monohydrate (COM) calculi [13] and that the pulsed-dye laser is not capable of fragmenting cystine calculi [3,4], the long-pulse Ho:YAG laser has been effective for all types of urinary calculi [1,14]. Ho:YAG lithotripsy has been so widely accepted that attempts have been made to design a smart laser lithotriptor for tissue selectivity and feedback control of energy [15].

However, the dominant mechanism by which calculi are fragmented by the Ho:YAG laser has not been well defined. The fragmentation process of calculi produced by nanosecond [16–18] Q-switched Nd:YAG laser (1.06 μm) and microsecond [17–19] pulsed-dye lasers (596 nm) is photomechanical and is described as laser-induced shockwave lithotripsy (LISL). The long-pulse Ho:YAG laser is not known to produce shock waves due to plasma expansion at the onset of laser irradiation [20–21]. In addition, the pres-

sure waves generated at cavitation collapse are speculated to have little contribution to fragmentation because of the weak pressure waves due to multiple collapses [20]. This is because the Ho:YAG laser generates elongated cavitation as a result of continuous deposition of laser energy at the base of the cavitation bubble due to the long pulse duration [22,23].

A fairly recent attempt by Dushinski et al. [7] to define the mechanism(s) of fragmentation by long-pulse Ho:YAG laser suggested a possible photothermal effect on urinary calculi. The authors reasoned that since experimental results showed no correlation between cavitation size (or fiber diameter) and lithotripsy efficiency, photomechanical effects (shock wave generated at cavitation collapse) could not be the dominant mechanism and therefore photothermal effects were assumed. However, these results did not delineate the photomechanical effect in fragmentation. In addition, the authors argued that the "glowing hot" stone fragments under water provided evidence of a photothermal effect. Schafer et al. [21] made the similar conclusion with their "dim whitish glow" and their measured emission spectrum that resulted in an unexpectedly high temperature (5,000 K). Although we support photothermal ablation as the probable damage mechanism, such a high blackbody temperature is unlikely.

In addition, Schafer et al. did not perform chemical analyses on the ablated calculi and its post-ablation water contents. In eliminating photomechanical effects as a damage mechanism, the authors also failed to provide sufficient evidence of acoustic transient, during which the delivery fiber was placed in parallel or perpendicularly in contact with the calculus surface. Instead, they replaced water with a low absorption liquid (acetonitrile; $\mu_a = 0.88\ cm^{-1}$ at 2.12 μm) to demonstrate the role of cavitation. Although we agree that vapor bubbles help disperse fragmentation, acetonitrile may not have provided the necessary environment for chemical breakdown of stone composition through reduction and oxidation as observed in clinical procedures. Instead, the authors only observed melting of the biliary stone by application of Ho:YAG under acetonitrile. Because the laser application was made in a quasi-anerobic environment, few if any further chemical degradation reactions occurred. Therefore, it is not surprising that they concluded a photothermal mechanism without any knowledge of possible chemical reactions.

On the other hand, both Schafer et al. and Dushinski et al. reported that fiber tips could be "welded" to the calculi upon holmium irradiation in the contact mode [7,21]. Dushinski et al. further noted that sulfur gas odor was detected during fragmentation of cystine calculi [7]. Zhong et al. [24] also reported that the fragmentation mechanisms differ for pulsed-dye laser and long-pulse Ho:YAG laser. Whereas LISL fragments are induced by shock waves, Zhong et al. observed that the holmium laser drills into the stone surface, a result of the well-known "Moses effect" [22].

These valuable observations suggested a dominant photothermal effect causing chemical decomposition of the calculus that warranted further verification. Previous experiments by Teichman et al. revealed that Ho:YAG lithotripsy created smaller fragments compared to pulsed-dye lasers [8], suggesting a different mechanism from LISL. Schafer et al. also observed that Ho:YAG irradiated calculus fragments appeared filamentary, indicating melting and re-crystallization, whereas those of LISL and mechanically crashed fragments were granular [21]. Also, radiant exposure and urinary-calculus compositions altered the efficiency of lithotripsy [9–10], leading us to believe that direct absorption of laser energy played a major role in calculus fragmentation as Schafer et al. suggested. The "Moses effect" seems to be a convenient model, which allows channeling of the holmium laser, and direct irradiation of and absorption by urinary calculi. Most recently, the discovery of cyanide as a result of laser-induced photothermal breakdown of uric acid calculus [11] confirmed the role of non shock wave ablative mechanism in long-pulse Ho:YAG lithotripsy.

In order to demonstrate that photothermal effects are the dominant mechanism behind Ho:YAG lithotripsy and erase the conventional wisdom that most if not all laser lithotripsies involve photomechanical stresses, we investigated the interaction of long-pulse Ho:YAG laser with a variety of urinary calculi. Several experiments were performed to demonstrate the dominantly photothermal-induced fragmentation process. First, fast-flash photography was used to capture images at different delay times with respect to the onset of the long-pulse Ho:YAG laser. This provided visualization of the lithotripsy event. Acoustical pressure measurements were recorded with a needle-hydrophone for analysis and correlation with images captured at different delay times. Mass-loss experiments were conducted with vari-

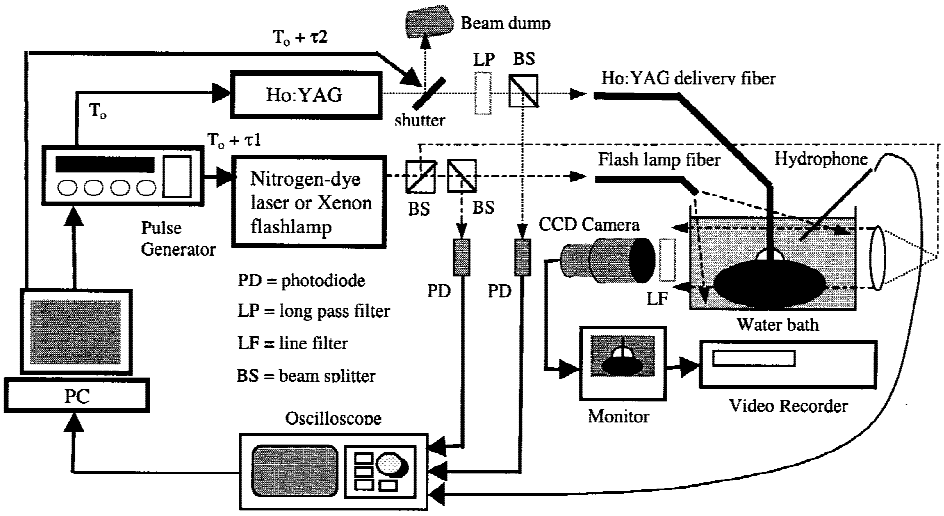

Fig. 1. Experimental setup for fast-flash photography and acoustic pressure measurement. A nitrogen-dye laser (λ = 540 nm) was used as a flashlamp initially for obtaining high quality (500-ps exposure time) time-resolved images. When no shock waves were observed, a broadband Xenon flashlamp (5-μs exposure time) was used in place of the nitrogen-dye laser, and a PVDF-needle-hydrophone was added during the pressure measurement experiment along with concurrent acquisition of fast-flash images.

ous urinary calculi in air (dehydrated and hydrated), and in water. The effects of initial calculus temperature on fragmentation were also investigated with fast-flash photography and mass-loss experiments. Finally, chemical analyses of calculus compositions pre- and post-irradiation were performed.

MATERIALS AND METHODS

Human urinary calculi were obtained from a stone analysis laboratory (Louis C. Herring Co., Orlando, FL). The calculi composed of either > 98% calcium oxalate monohydrate (COM), > 98% calcium hydrogen phosphate dihydrate (CHPD), > 98% magnesium ammonium phosphate hexahydrate (MAPH), > 98% cystine, or > 98% uric acid. The experiments were performed either with a Laser 1-2-3 from Schwartz Electro-Optics (λ = 2.12 μm, 250– 350 μs) at the University of Texas at Austin, or with a VersaPulse Select from Coherent Medical Group (λ = 2.12 μm, 250 μs) at the University of Texas Health Science Center at San Antonio. Except for the experiments comparing calculus mass-loss in air (dehydrated and hydrated calculi) and in water, where a 365-μm diameter low OH^- fiber (Simline-365, Coherent Medical Group, Palo Alto, CA) was used, all other experiments were conducted with a 550-mm diameter low OH^- fiber (Simline-550, Coherent Medical Group).

Six experiments were conducted to elucidate the mechanisms of long-pulse Ho:YAG lithotripsy of urinary calculi:

(1) Fast-flash photography of laser-calculus interaction (COM and cystine; UT Austin);
(2) Pressure transient measurements with a PVDF needle-hydrophone (COM and cystine; UT Austin);
(3) The effect of fiber orientation on lithotripsy (COM and cystine; UT Austin);
(4) Mass-loss measurements of calculi in air (dehydrated and hydrated calculi) and in water (COM; UTHSC San Antonio);
(5) The effect of initial calculus temperature on fragmentation or mass-loss (UTHSC San Antonio);
(6) Chemical analysis of calculus composition pre- and post-irradiation (COM, CHPD, cystine, MAPH, and uric acid calculi; UTHSC San Antonio).

Fast-Flash Photography of Laser-Calculus Interaction

Fast-flash photography was performed to monitor the dynamics of laser lithotripsy on two types of urinary calculi: COM and cystine. In this experiment, the calculi were cut with a dental diamond band saw to provide a flat target surface. A calculus was then placed in a water-filled glass cuvette at room temperature (~ 23°C). During lithotripsy, the delivery fiber was placed at three orientations; either perpendicular, at a 45° angle, or parallel to the calculus surface.

The setup for fast-flash photography is shown in Figure 1. A 100-MHz computer (Gateway 2000, North Sioux City, SD) with a LabVIEW controlled data acquisition software package was used to trigger a pulse generator (DG535, Stanford Research Systems, Sunnyvale, CA), which in

turn controlled the delay time between the onset of the Ho:YAG laser pulse and the nitrogen-dye laser pulse (LN-1000 nitrogen gas laser and LN-102 dye module, Laser Photonics, Orlando, FL; τ_p = 500 ps; λ = 540 nm).

A long pass filter (03-FCG-113, Melles Griot, Irvine, CA) was used to prevent contamination of our images by blocking visible and near infrared wavelengths (< 1,000 nm) emitted from the Ho:YAG laser flashlamp, which consistently produced bright "glow" due to scattering. The holmium laser beam was coupled into a 550-μm low OH^- optical fiber to be delivered to the calculus in a water bath. Two beam splitters were placed at the outputs of the long-pulse Ho:YAG laser and the nitrogen-dye laser to couple a small fraction (~ 4%) of the laser energies to two photodiodes. Signals generated from the photodiodes, representing the temporal beam profiles of the lasers, were monitored on a digital oscilloscope (TDS-640A 500 MHz-200 GS/s, Tektronix, Beaverton, OR). Knowing the exact relative temporal displacement between the two lasers allowed us to determine the delay time of our fast-flash images from the onset of the Ho:YAG laser pulse.

The nitrogen-dye laser (500-ps exposure time) was used as the light source for fast-flash photography (A Xenon flashlamp was used in place of the nitrogen-dye laser for a later experiment). This light source was split into two beams for simultaneous reflectance and transmission imaging. A series of delay times was used to record lithotripsy events. A line filter (03-FIV-113, Melles Griot, Irvine, CA) at (540 ± 10) nm was placed in front of the CCD camera (GP-MF 602, Panasonic, Japan), allowing only the nitrogen-dye wavelength to be transmitted into the CCD array. This technique further enhanced our imaging capability by avoiding contamination from the Ho:YAG laser flashlamp. The images captured by the CCD camera were recorded on a VCR (HR-S5200U, JVC, Japan) and displayed on a video monitor. A time counter (TG-50, Horita, Mission Viejo, CA) was used to label the images as they were recorded. From the videocassette, individual frames of images were analyzed in freeze-frame style on a video monitor or with a frame-grabber (Snappy, Play Incorporated, Rancho Cordova, CA) on a computer monitor.

Before each experiment, both ends of the optical fiber were cleaved and polished. The output energy from the delivery fiber was measured by a power meter (EPM-2000 powermeter, and J25 series pyroelectric joulemeter, Molectron Detector, Inc., Portland, OR). The energy employed in this experiment was maintained at 375 ± 5 mJ/pulse for a pulse duration of 250 μs. During the experiment, nine warm-up Ho:YAG laser pulses (1.5–2.0 Hz) were delivered to a beam dump with a mirror shutter to allow the laser to achieve a stable energy level. The tenth and final pulse was delivered to the target calculus in the water bath by removing the shutter from the beam path. The nitrogen-dye laser pulse was then triggered at a pre-set delay time from the onset of the final Ho:YAG laser pulse. A sequence of laser pulses and delay times provided images of the complete dynamic lithotripsy event, extending to hundreds of microseconds after the end of the Ho:YAG laser pulse. At least five images were captured for each delay time for the COM calculus and the cystine calculus at each different fiber orientation; either perpendicular, at a 45° angle, or parallel to the calculus surface.

Pressure Wave Measurements

The laser-induced pressure transients were measured using a PVDF needle-hydrophone, which consisted of a piezoelectric polyvinylidene-fluoride foil as its active element (40-ns rise time, 1.502 mV/bar, where 1 bar ≈ 10^5 Pa ≈ 1 atm, Imotec Messtechnik, Germany). Pressure measurements were conducted for three different configurations: (1) ablation in clear water, (2) ablation with delivery fiber perpendicular to calculus surface in contact mode, and (3) ablation with delivery fiber parallel to calculus surface in contact mode. The hydrophone was placed a few millimeters away from the calculus surface to avoid possible damage due to ejected fragments. Ho:YAG irradiation was delivered via a 550-μm low OH^- fiber. An energy of 400 mJ/pulse (2.5 Hz) at 350-μs pulse duration was used. The signal from the hydrophone was displayed and recorded on a digital oscilloscope (Tektronix TDS 640A). Later, the signals were analyzed and back-calculated to a pressure transient 1-mm away from the origin of bubble collapse. At the same time, images were captured using fast-flash photography at different delay times with respect to the onset of the Ho:YAG pulse. These images provided concurrent information on the dynamics of cavitation bubbles or lithotripsy. The setup for this experiment was the same as the fast-flash photography experiment (Fig. 1), but with an additional needle-hydrophone in the water bath and a Xenon flashlamp (5-μs exposure time) in place of the nitrogen-dye laser. The nitrogen-dye laser was used

in the previous experiment to image possible shock waves induced by the holmium laser with its short exposure time (500 ps), but was replaced with the less tedious Xenon flashlamp when no plasma-induced shock wave was discovered by photography and pressure measurements. At least five pressure measurements were recorded for each configuration mentioned above.

Comparison of Fiber Orientation

COM calculi were sandpapered to obtain a flat surface, cleaned, and dried for a few hours. An image was then captured with a CCD camera as a control. After hydrating the stones for a few hours, the experiment was then conducted in two configurations: (1) a fiber placed parallel to the calculus surface with the side of the fiber in contact with the calculus, and (2) a fiber placed perpendicular to the calculus surface with the fiber tip in contact with the calculus. After ablation for approximately 330 seconds (400 mJ/pulse at 2.5 Hz), the calculi were removed from the water bath and left to dry. Images of the resulting pits or craters were captured again with the CCD camera and their dimensions were estimated with a caliper.

Mass-Loss Measurements

Prior to laser irradiation, all COM calculi involved in mass-loss measurements were dehydrated by placing the samples in a –80°C freezer for 24 hours. The samples were then desiccated for another 24 hours in a vacuum lyophilizer to reduce humidity. Initial calculus mass was measured after desiccation. The calculi were randomly divided into three groups for contact lithotripsy (1) in air after submerging in water for 24 hours—"hydrated calculus in air," (2) in water after submerging in water for 24 hours, and (3) in air after storage within the lyophilizer for 24 hours—"dehydrated calculus in air."

Each calculus was irradiated with 150 J holmium energy (0.5 J/pulse at 8 Hz) via a 365-μm low OH^- optical fiber. The fiber tip was cleaved prior to lithotripsy of each calculus. The calculi were ablated with fiber contact using a scanning mode along the surface. This helped preserve the "parent" calculus by preventing it from being fragmented into several large "sister" calculi, which might cause difficulty during mass-loss measurements. A total of 13 measurements for submerged calculi, 14 measurements for "hydrated calculi in air," and 18 measurements for "dehydrated calculi in air" were performed.

After lithotripsy, the calculi ablated in water were centrifuged at 2,000 rpm for 20 minutes. The supernatant was then discarded, and the pellet was placed in a –80°C freezer for two hours. Calculi from all groups were desiccated once again with a vacuum lyophilizer before the final calculus mass was measured. Calculus mass-loss was defined as the difference between the initial calculus mass and the final calculus mass of the remaining "parent" calculus.

Effects of Initial Calculus Temperature on Fragmentation

The effects of initial calculus temperature were determined in terms of mass-loss. This study was performed using COM and cystine calculi by qualitatively comparing the mass-loss of pre-cooled calculi taken from a –80°C freezer and with that of uncooled calculi at room temperature. The initial mass was measured on both pre-cooled and uncooled calculi. Each calculus was then irradiated in contact with a 550-μm low OH^- optical fiber using single 1.0-J holmium pulses at 20 separate locations with the scanning mode. The final mass for each calculus was measured. The measurements were based upon five samples of each calculus types at either the pre-cooled or uncooled temperature. Again, mass-loss was defined as the difference between the initial mass prior to lithotripsy and the final mass post-lithotripsy.

Pre- and Post-Irradiation Chemical Analysis

A set of Ho:YAG pulses with a total energy of 200 J (1 J/pulse at 10 Hz) was delivered using a 550-μm low OH^- optical fiber to various calculus types including COM, CHPD, MAPH, cystine, and uric acid. At least three samples of each calculus types were used to perform this series of experiments. After irradiation, composition analyses were performed separately for the parent calculi, the calculus craters, fragments $\geq$ 710 mm, and fragments < 710 mm. Composition analyses of all fragments were performed using infrared spectroscopy and x-ray crystallography at the same calculus laboratory where initial calculus composition analyses were performed. The laboratory was asked to look for thermal products for each of the calculi (Table 1).

For cystine, the parent calculus, the fragments, and the water in which lithotripsy was performed were analyzed. Electron impact ionization mass spectra were acquired on a Finnigan MAT 4615 quadrupole mass spectrometer (Finnigan, Palo Alto, CA) at an electron energy of 70 eV

TABLE 1. Dehydration, Decomposition, or Conversion Temperatures for Various Urinary Calculi, and Their Products [40].

Composition	Temperature (°C)	Decomposition products
Calcium oxylate monohydrate (COM)	206	Calcium carbonate
Calcium hydrogen phosphate dihydrate (CHPD)	109	Calcium phyrophosphate
Cystine	264	Free sulfur, cysteine[a]
Magnesium ammonium phosphate hexahydrate (MAPH)	100	Dehydrates
Uric acid	Temperature unspecified	Cyanide

[a]Cysteine has a boiling point lower than cystine melting point.

and an ion source temperature of 160°C. Sample introduction was by means of a direct insertion probe that was heated ballistically until evaporation was complete. Electrospray ionization mass spectra were obtained on a Finnigan MAT LCQ ion trap mass spectrometer. Samples were dissolved in 2% triofluoroacetic acid and diluted with 50% aqueous acetonitrile containing 0.5% acetic acid to reach a final concentration of 0.5 pmole/μl. Sample introduction was by direct infusion into the mass spectrometer at a flow rate of 10 μl/min. The charge-state of each ion of interest was determined through the Zoom Scan feature of the LCQ. MS/MS spectra were obtained for each analyte and compared to reference standards in order to confirm identification.

For uric acid, a standard micro-diffusion assay was used, in which cyanide is trapped in alkali, and reacted with pyridine and barbituric acid to form a color complex that is measured by spectrophotometry [25]. Because of the clinical significance of cyanide, three separate uric acid calculi were irradiated and sent to three separate toxicology laboratories for analysis.

RESULTS

Fast-Flash Photography of Laser-Calculus Interaction

In this experiment, fast flash images on the dynamics of cavitations and laser lithotripsy were captured with the holmium laser set at 375 mJ/pulse for a pulse duration of 250 μs. With the delivery fiber suspended in clear water and the urinary calculus (COM or cystine) located at a distance of ~ 5 mm away from the fiber tip, an elongated vapor bubble was produced that did not reach the calculus. No fragmentation was visible at any time. When the delivery fiber was advanced to within 1 mm of the calculus surface, lithotripsy occurred if and only if the expanding bubble reached the surface of the calculus. Because of the long pulse duration, laser energy propagated through the vapor channel of the bubble and was directly absorbed on the calculus surface. This off-contact lithotripsy produced few fragments with a large hemispherical bubble that expanded to its maximum size around 250 μs and collapsed around 450 μs after the onset of the holmium laser pulse (Figure 2A–D). No fragmentation was observed after the bubble collapsed.

With the delivery fiber placed in contact and perpendicular to the calculus surface, fast-flash photography of COM and cystine calculi showed lithotripsy began after about 50 μs, as illustrated in Figure 3, when a plume formation consisting of dust or fragments and bubbles appeared. The plume continued to enlarge, and reached its maximum expansion at approximately 200 μs and 400 μs for the COM and cystine calculi, respectively, as shown in Figure 4A and 4B. No lithotripsy attributable to pressure wave expansion in the early stage of bubble formation or in the later stage of bubble collapse was observed. When the fiber was placed at a 45° angle in contact mode, the Ho:YAG laser produced a distorted bubble and a smaller plume with less fragmentation (Figure 5A–C). Again, no fragmentation was seen at either the onset of the holmium laser or after bubble collapse.

When the delivery fiber was placed in contact but parallel to the calculus surface, no fragmentation was observed during bubble expansion or collapse. Figure 6 illustrates that an elongated half-bubble was formed along the surface of a COM calculus. It reached maximum expansion at 350 μs (Fig. 6A) and collapsed between 450 and 550 μs (Fig. 6B) after the initiation of the Ho:YAG

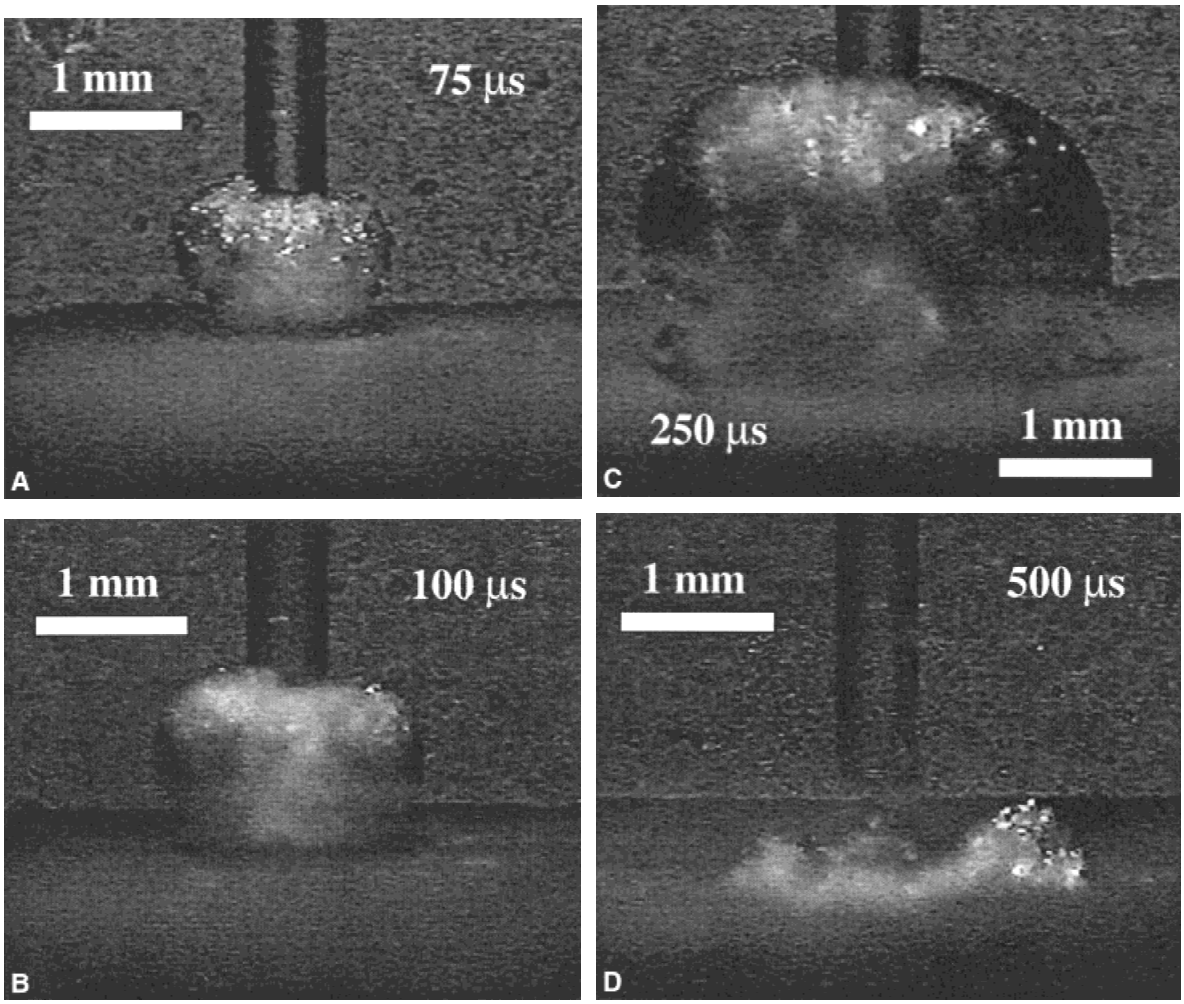

Fig. 2. These images illustrate noncontact holmium laser lithotripsy: **A:** At 50 to 75 μs, the expanding vapor bubble (glassy appearance) reaches the calculus surface. Lithotripsy occurs upon penetration of holmium energy through the vapor channel to the exposed calculus surface. At 100 μs, **B:** The vapor bubble becomes more "dusty" due to thermal breakdown of calculus compositions and fragmentation. At 250 μs, **C:** The maximum expansion of the vapor bubble occurs with more fragmented dusts. After bubble collapse, shown here at 500 μs, the plume disperses and no further fragmentation is observed **D:** Holmium laser energy was set at 375 mJ/pulse for 250-μs pulse duration.

laser pulse. Beyond 600 μs (Fig. 6C), no plume or fragmentation ejecting from the calculus surface was apparent.

Pressure Wave Measurements

A typical temporal profile of the Ho:YAG laser pulse (400 mJ/pulse, 350 μs) and the corresponding pressure transients for COM and cystine calculi are shown in Figures 7 and 8, respectively. The pressure transients were corrected to 1 mm away from the center of the bubble or cavitation collapse. The figures also illustrate the relative collapse time of cavitations created in water through the fiber in three configurations: (1) in clear water, (2) with the fiber placed perpendicular to the calculus surface, and (3) with the fiber placed parallel to the calculus surface.

According to our pressure transient data, a typical vapor bubble in clear water collapsed within 400–450 μs after the onset of a 400-mJ laser pulse energy (Figs. 7A and 8A). However, a bubble induced with the fiber placed parallel to the stone surface collapsed later between 450 μs and 550 μs (Figs. 7C and 8C), indicating that the bubble was distorted or larger in at least one dimension. Our fast-flash images confirmed this observation. The bubble induced when placing the fiber parallel to the calculus surface was more elongated than that in clear water. This was because the calculus surface obstructed the bubble's

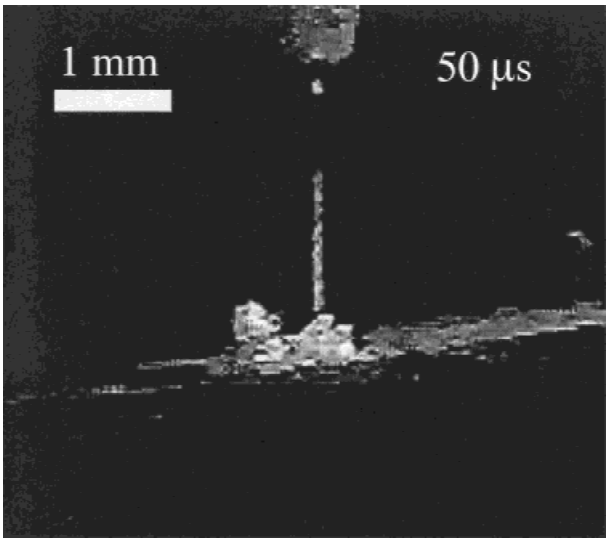

Fig. 3. For contact-mode, holmium lithotripsy begins at 50 μs after the onset of the holmium laser. This discovery does not agree with conventional knowledge of LISL, whereby lithotripsy occurs by shock wave generation during plasma expansion in nanosecond Nd:YAG laser less than 1 μs after the onset of the laser, and during cavitation collapse in microsecond pulsed-dye laser more than 200 μs after the onset of the laser, respectively. Pressure measurements did not reveal any shock wave during bubble expansion and only a pressure wave on the order of 2 bars were detected at 1-mm distance from the location of cavitation collapse at 300 μs for COM calculus. Holmium laser energy was set at 375 mJ/pulse for 250-μs pulse duration.

radial expansion, so it expanded more axially. This configuration did not produce fragmentation, as proven by an image captured after the bubble had collapse at about 600 μs, shown in Figure 6C. The pressure peak due to the collapse was less than 20 bars, and did not induce any photomechanical damage to the urinary calculus.

When lithotripsy was performed with the fiber perpendicular to the calculus surface, a pressure transient indicating a small pressure peak of about two bars for the COM stone occurred upon bubble collapse at 300 μs (Fig. 7B). Irradiation of the cystine stone produced pressure fluctuations of less than one bar, with no apparent pressure peak due to cavitation collapse (Fig. 8B). However, plume formation began approximately 50 μs after the initiation of the Ho:YAG pulse as reported previously, and reached its maximum around 150–200 μs (Fig. 4A and 9A) for the COM calculus before any pressure peak was observed, and around 400 μs for the cystine calculus. Images captured on the COM stone just after the small pressure peak (~ 2 bars; Fig. 9B) at 300 μs show barely visible fragmentation due to cavitation collapse. This illustrates, again, that the

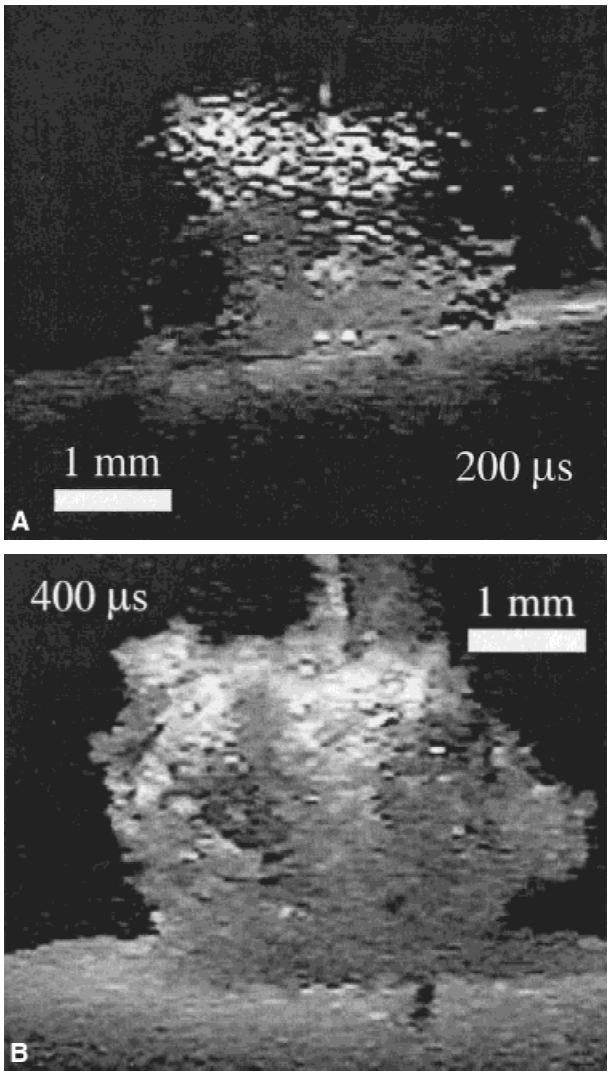

Fig. 4. Maximum expansion of "plume" formation, a mixture of vapor bubble and dust containing calculus fragmentation upon thermal breakdown of **A:** COM, and **B:** Cystine calculi. Holmium laser energy was set at 375 mJ/pulse for 250-μs pulse duration.

pressure wave induced by cavitation collapse, or by a presumed photomechanical mechanism is not responsible for significant calculus fragmentation by the long-pulse Ho:YAG laser.

Comparison of Fiber Orientation

When a COM calculus was ablated with the fiber parallel to its surface in water for 330 seconds with 400 mJ/pulse at 2.5 Hz, a small pit (~ 1 mm diameter and < 0.5 mm deep) resulted (Fig. 10B). On the contrary, when a COM calculus was ablated with the fiber placed perpendicularly to its surface, a large crater was pictured with the CCD camera. The crater measured approximately

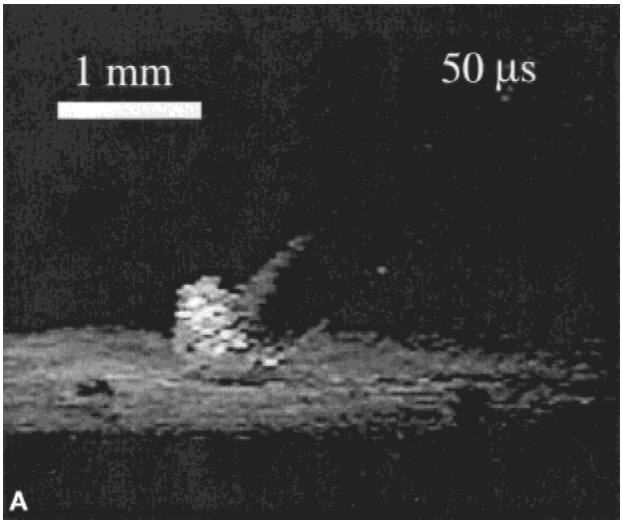

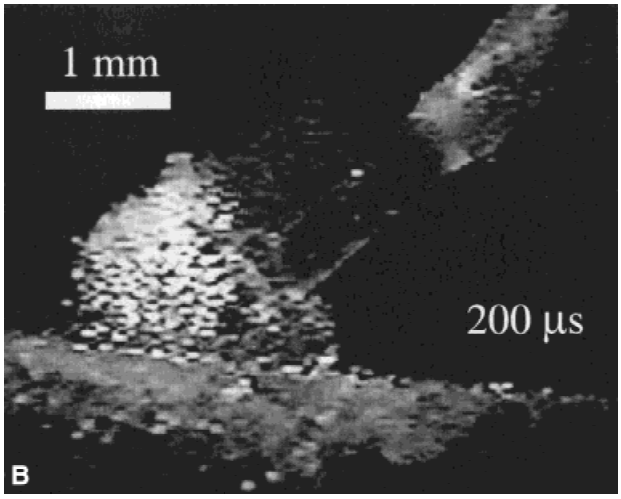

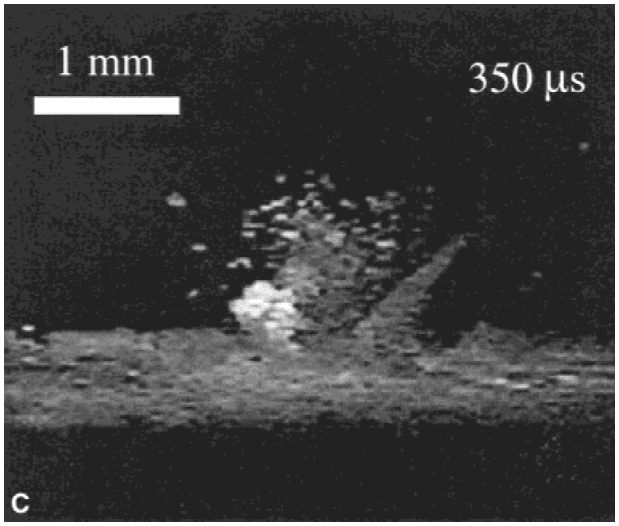

Fig. 5. Holmium lithotripsy at 45-degree angle: **A:** Shows bubble expansion at 50 μs. **B:** Shows that the maximum expansion of the vapor bubble and the fragmented dust is comparatively much less than that in contact-mode. **C:** Upon collapse at 350 μs, only small fragments continued to be ejected from the ablated site. Holmium laser energy was set at 375 mJ/pulse for 250-μs pulse duration.

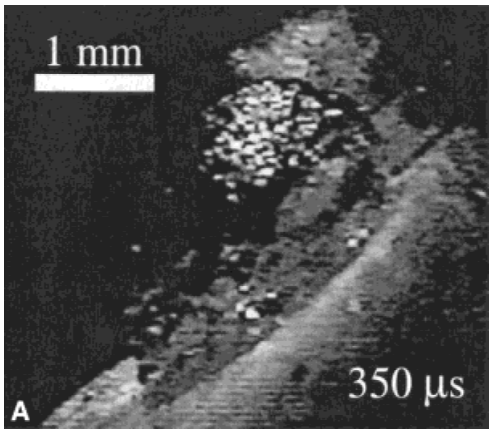

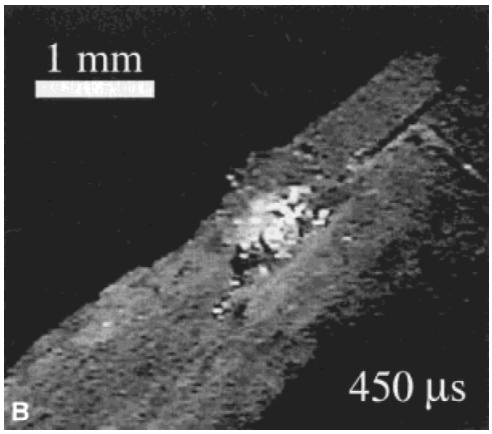

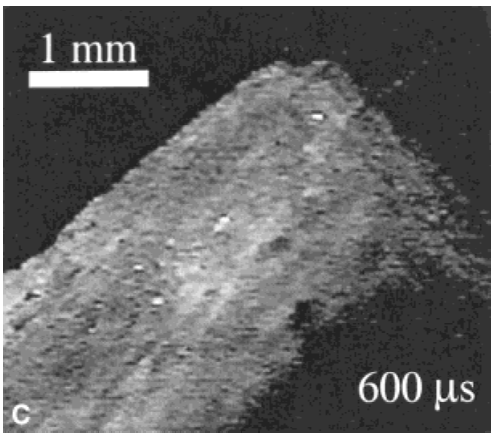

Fig. 6. Holmium lithotripsy with parallel fiber orientation along the urinary calculus. **A:** Illustrates the half-sized elongated vapor bubble at its maximum expansion around 350 μs. Upon cavitation collapse around 450 μs **B:** A pressure wave on the order of 20 bars was detected, but no fragmentation occurred thereafter, **C.** Holmium laser energy was set at 375 mJ/pulse for 250-μs pulse duration.

5 mm in width and about 2 mm in depth, as shown in Figure 10C.

Mass-Loss Measurements

Calculi were divided into three groups for mass-loss measurements where there was no sta-

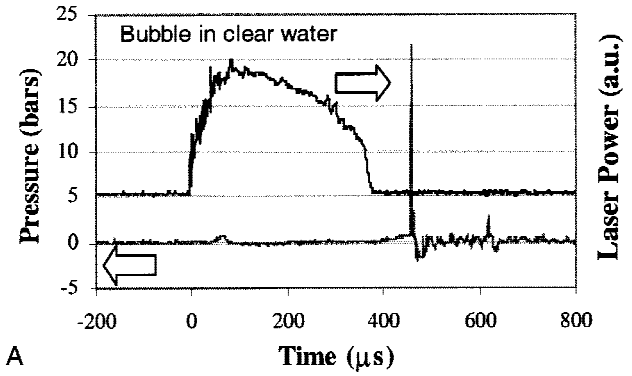

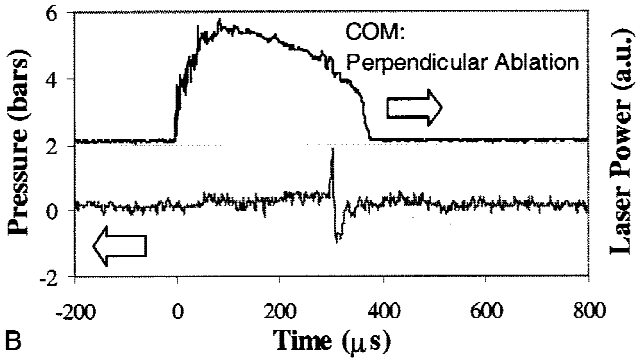

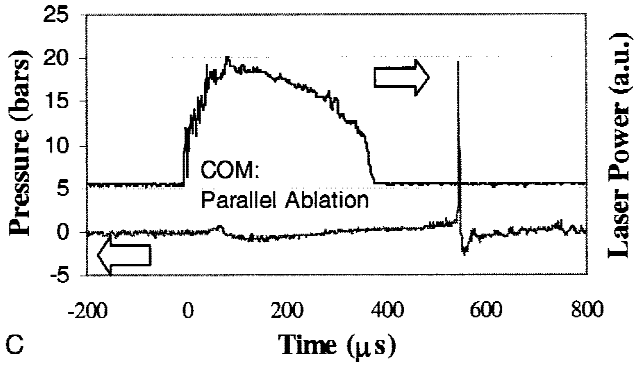

Fig. 7. Time profile of the holmium laser pulse (top) and the measured pressure for each figure. **A:** Bubble only: Ho:YAG laser pulse begins at 0 μs. A small pressure bump characteristic of long-pulse mid-infrared laser was detected after laser onset. Bubble collapse occurred at 450 μs inducing a pressure peak >20 bars (typically above 15 bars), rebounded, and recollapsed at about 600 μs. **B:** Perpendicular ablation on COM: Ho:YAG laser pulse begins at 0 μs. Upon cavitation collapse, a small pressure peak about 2 bars was detected at around 300 μs. **C:** Parallel ablation on COM: Ho:YAG laser pulse begins at 0 μs. A pressure peak <20 bars at 545 μs (range: 450 to 600 μs) was detected; sometimes a second pressure peak occurred. Holmium laser energy was set at 400 mJ/pulse for 350-μs pulse duration.

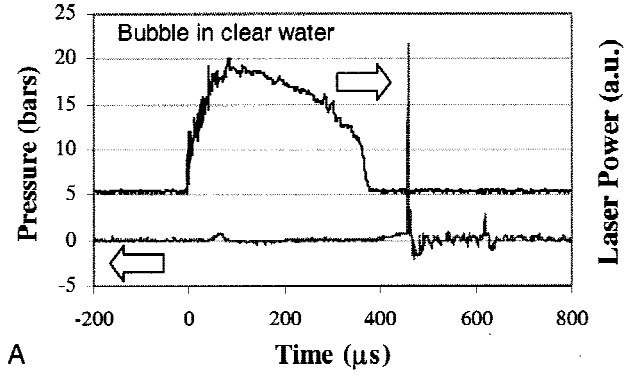

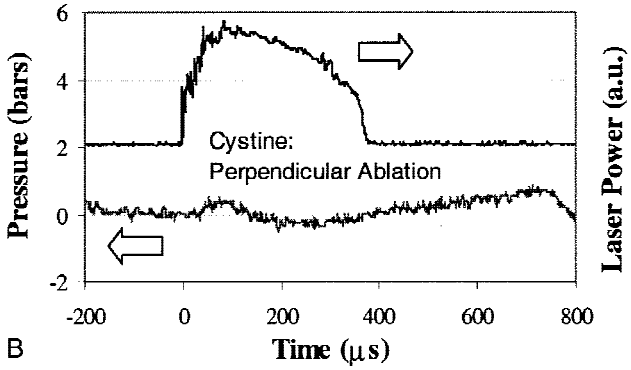

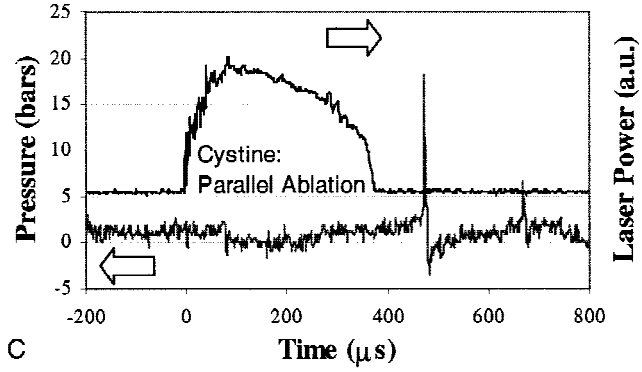

Fig. 8. Time profile of the holmium laser pulse (top) and the measured pressure for each figure. **A:** is the same as Figure 7A; shown here for ease of comparison. **B:** Perpendicular ablation on cystine: Ho:YAG laser pulse begins at 0 μs. No significant pressure peak was observed (~1 bar). **C:** Parallel ablation on cystine: A pressure peak was detected at 475 μs (<20 bars typical and occurred in the range of 450 to 500 μs); a second pressure wave occurred at about 700 μs. Holmium laser energy was set at 400 mJ/pulse for 350-μs pulse duration.

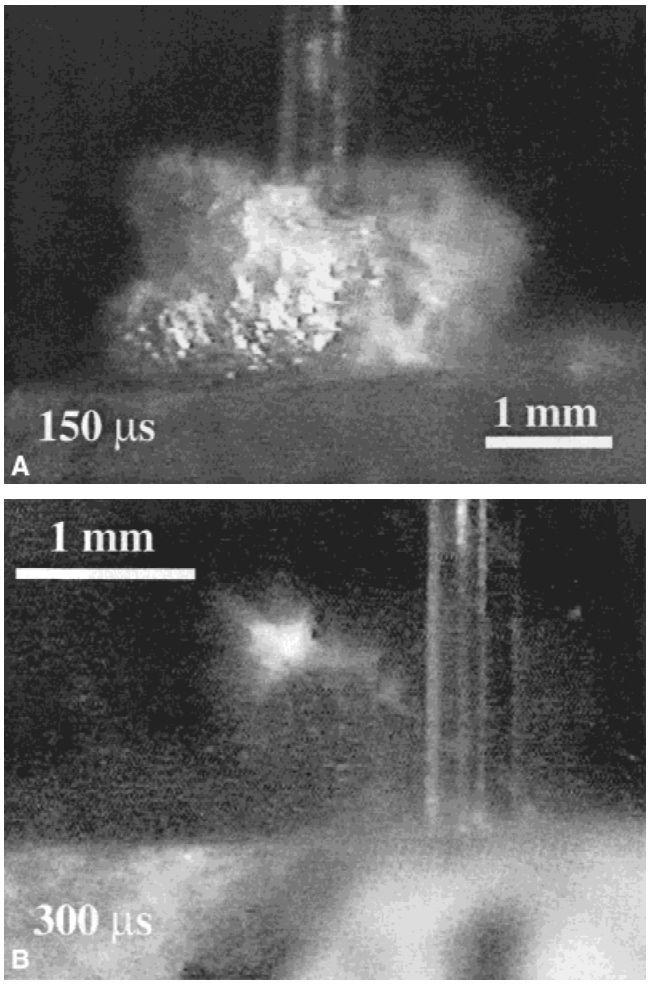

Fig. 9. Illustrates that holmium lithotripsy occurred prior to cavitation collapse. **A:** Shows a maximum plume formation at 150 μs after laser onset on a COM calculus. **B:** Shows no further fragmentation upon bubble collapse at about 300 μs. Holmium laser energy was set at 400 mJ/pulse for 350-μs pulse duration.

tistically significant pairwise difference in the initial average mass of each group. With the previously mentioned laser parameters, calculus mass-loss was significantly greater for dehydrated calculi in air than for hydrated calculi in air, and both were greater than the mass-loss for calculi submerged in water. Analysis indicated that, with $P < 0.001$, there was statistical significance among the results of the three experimental configurations (Table 2).

Effects of Initial Stone Temperature on Fragmentation

From Table 3, it can be seen that mass-loss was significantly lower for pre-cooled COM and cystine calculi (2.2 ± 0.9 and 0.8 ± 0.4, respec-

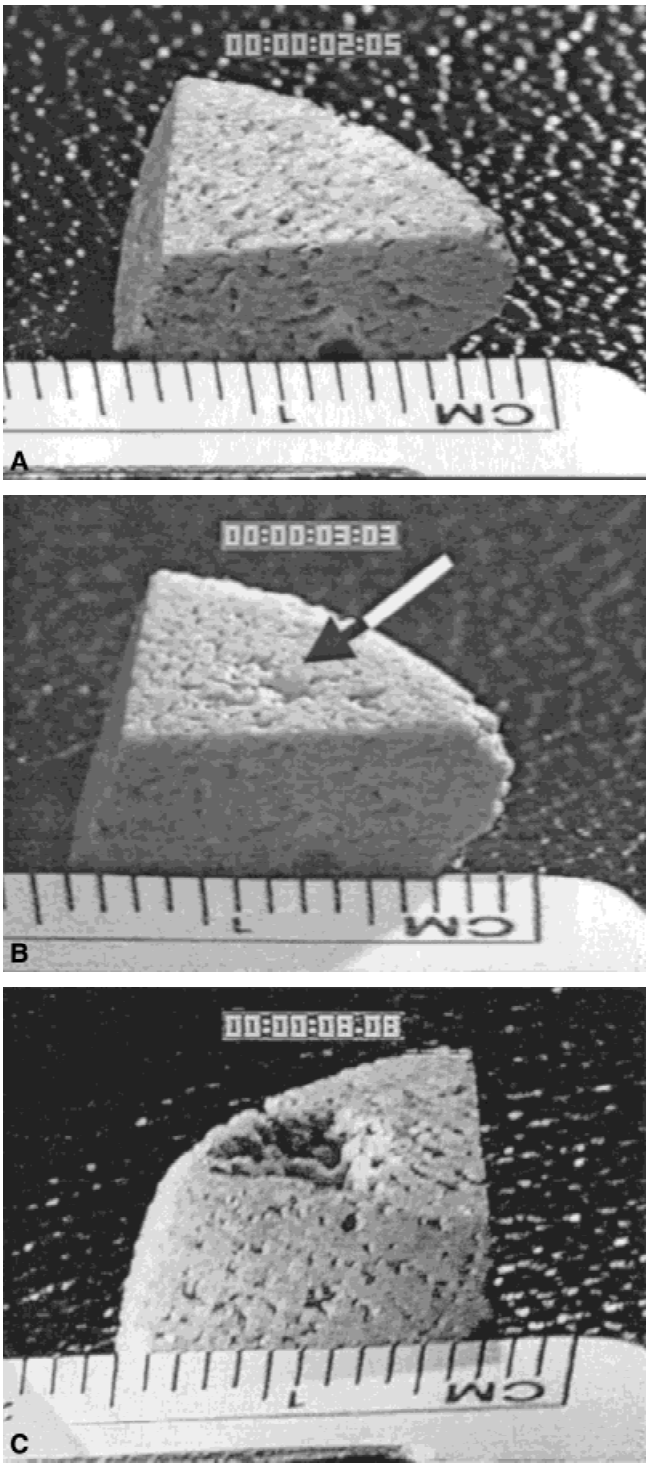

Fig. 10. **A:** Shows the control image prior to holmium lithotripsy in water. With a parallel fiber orientation in contact with the calculus surface, **B,** no significant fragmentation occurred after delivery of 330 J of holmium energy. With a perpendicular fiber orientation in contact-mode, **C,** however, lithotripsy occurred leaving behind a crater measuring 5-mm in width and 2-mm in depth.

TABLE 2. COM Calculus Mass-Loss (mg, Mean ± Standard Deviation) for a Total of 150-J Ho:YAG Energy (0.5 J/pulse at 8 Hz)[a]

	Calculi in water (n = 13)	Hydrated calculi in air (n = 14)	Dehydrated calculi in air (n = 18)	*P*-value
Pre-Ablation calculus mass	141 ± 22	128 ± 48	118 ± 78	0.8
Post-Ablation calculus mass-loss	17 ± 3	25 ± 9	40 ± 12	0.001

[a]Pairwise comparisons were statistically significant at an $\alpha \leq 0.01$ for calculi in water vs. hydrated calculi in air and dehydrated calculi in air; and for hydrated calculi in air vs. dehydrated calculi in air.

TABLE 3. Mass-Loss (mg, Mean ± Standard Deviation) for COM and Cystine Calculi at a Pre-Cooled Temperature (> –80°C) and at Room Temperature (~ 23°C), in Air

	Pre-cooled temperature (> –80°C) (n = 5)	Room temperature (~ 23°C) (n = 5)	*P*-value
Calcium oxylate monohydrate (COM)	2.2 ± 0.9	5.2 ± 1.6	0.02
Cystine	0.8 ± 0.4	2.2 ± 1.1	0.05

tively) compared to uncooled COM and cystine at room temperature (5.2 ± 1.6 and 2.2 ± 1.1, respectively).

Pre- and Post-Irradiation Chemical Analysis

For COM, the parent calculi and fragments ≥710 μm showed no change in composition. The fragments < 710 μm were a combination of calcium carbonate and COM. For CHPD calculi, no chemical changes were detected in the parent calculi and fragments ≥ 710 μm. CHPD crater surfaces showed amorphous calcium phosphate (carbonate apatite and hydroxylapatite), whereas fragments < 710 μm showed CHPD, amorphous calcium phosphate, and calcium pyrophosphate. For MAPH calculi, no chemical change was found in the parent calculi. MAPH crater surfaces, fragments ≥710 μm, and fragments < 710 μm showed MAPH and the presence of ammonium carbonate and magnesium carbonate.

For cystine calculi, all fragments remained as cystine. The water in which cystine lithotripsy was performed, however, showed the presence of free sulfur. With electron impact ionization mass spectrometric (EI/MS) analysis, substantial quantities of free sulfur and minute traces of cysteine in the aqueous medium above the laser-treated calculi were detected. There was no evidence of either free sulfur or cysteine in a washed sample of the remaining solid material after laser irradiation. Likewise, there was no free sulfur or cysteine in untreated calculi. By electrospray ionization mass spectrometry (ESI/MS), it was observed that only cystine was present in the washed laser-treated calculus residue and that the supernatant contained predominantly cystine along with very low levels of cysteine.

For uric acid calculi, all fragments recovered were uric acid. However, the water in which uric acid lithotripsy was performed indicated the presence of cyanide in all specimens. This cyanide test was repeated at three separate toxicology laboratories with consistent results.

DISCUSSION

It is well documented that shock wave-induced fragmentation occurs during plasma expansion and upon bubble collapse in Q-switched Nd:YAG and pulsed-dye laser lithotripsies [16–19], respectively. In nanosecond Q-switched Nd:YAG lithotripsy, both plasma expansion and bubble collapse generate shock waves with magnitudes in excess of 100 bars. These shock waves result in instantaneous fragmentation as they traverse the calculus surface and mechanically couple their energy to the target. In microsecond pulsed-dye laser lithotripsy, fragmentation occurs only upon bubble collapse because the microsecond pulse duration creates a delayed plasma expansion and a smaller initial shock wave.

In this study, no fragmentation was observed in fast-flash images during the early stages of bubble expansion or upon bubble collapse. The long-pulse Ho:YAG laser did not generate shock waves or pressure waves on the order of magnitude necessary to contribute to fragmentation. Concurrent pressure measurements indicated that maximum fragmentation of the COM and cystine calculi was not a consequence of shock

wave impact (Fig. 4 and 9A). With COM calculi, only a small pressure wave (< 2 bars, Fig. 7B) was recorded upon bubble collapse. No pressure wave was detected for cystine calculi except for a small pressure transient (< 1 bar, Fig. 8B). However, when a 20-bar pressure wave (Figs. 7C and 8C) was recorded during bubble collapse for a parallel fiber along the calculus surface, no fragmentation was observed in fast-flash images. If shock waves produced by plasma expansion or bubble collapse resulted in lithotripsy, the parallel fiber orientation would have caused fragmentation, since shock waves propagate spherically in all directions [16–20]. This suggests that during routine Ho:YAG clinical use, urinary calculus fragmentation is not shock wave-induced [21].

On the other hand, there was evidence that lithotripsy occurred by direct absorption of laser energy by the calculus. It was observed that lithotripsy only began when the "Moses effect" [22–23] allowed channeling of the laser beam through the vapor bubble to the calculus surface (Fig. 2). The absorption coefficient, μ_a, of Ho:YAG laser in water was 25 cm^{-1} associated with 1/e of light penetration according to Beer's Law; the penetration depth, $1/\mu_a$, was 400 μm [26]. In the absence of stress confinement in the medium because of the long laser pulse duration [20,23,27–29], a layer of water 400 μm in depth was evaporated rapidly upon irradiation without plasma expansion or shock wave generation. The conversion of water into vapor created an expanding vapor bubble beneath the delivery fiber. Since the density of vapor is 1,672 times less than that of water (at 100°C, ρ_{water} = 1,000 g/cm^3 and ρ_{vapor} = 0.598 g/cm^3), the absorption coefficient of vapor was reduced proportionally to about 0.015 cm^{-1}. Hence, the vapor bubble acted as a channel allowing continuous laser energy transmission to the exposed calculus surface.

In the early phase of our research, we consistently observed the hot or whitish "glow" [7,21]. Upon identifying this "whitish glow" as scattered light originating from the holmium flashlamp, we placed a long pass filter (1,000 nm) at the output coupler of the laser cavity to eliminate the Xenon arc emission that was delivered through the clinical fiber along with the holmium energy. As can be seen, all fast flash images (Figs. 2–6) captured did not show the presence of a hot "glow" at the laser pulse energies used to perform our experiments. Xenon arc lamps are the commonly used holmium pumps and are known to have a blackbody temperature of 5,200 K [30]. If care is not taken, the "whitish glow" can easily be mistaken as a result of holmium-calculus interactions.

Previous studies have shown that bubble collapse does not necessarily result in shock wave or significant pressure wave formation [20,24,29]. This is because long-pulse mid-infrared lasers like the Ho:YAG laser produce pear-shaped or elongated vapor bubbles that eventually terminate with multiple collapses instead of spherical bubbles that collapse to a point. These multiple collapses weaken the mechanical coupling efficiency of the bubble, generating only weak pressure waves.

Experimental results (Figs. 7C and 8C) show that the maximum pressure wave (~ 20 bars) was generated when the delivery fiber was parallel to the surface of the calculus. This pressure amplitude was significantly larger than that recorded when the delivery fiber was placed in contact and perpendicular to the target, as in a typical clinical procedure (P < 2 bars, Figs. 7B and 8B). Upon bubble collapse, however, no fragmentation was detected (Fig. 6C) and no effective lithotripsy was recorded after delivery of 330-J laser energy (Fig. 10B). Only a small pit was visible in Figure 10B, most likely a result of the diverging laser beam from the delivery fiber (large numerical aperture) and a wallward jet [31–34] upon bubble collapse. These data rule out stone ablation through photomechanical or photoacoustical mechanisms, consistent with the observation made by Beghuin et al. that vapor bubbles have "a minimal incidence on stone fragmentation" [29].

Chemical analyses of various urinary calculi post-lithotripsy consistently revealed thermal breakdown components (Table 1). Unlike LISL where 22 mJ of nanosecond Q-switched Nd:YAG and 100 mJ of microsecond pulsed-dye laser energies were enough to create fragmentation by means of shock wave coupling, the long-pulse Ho:YAG laser has to operate above the calculus threshold ablation in order for lithotripsy to occur. Although these threshold energy levels have not been quantified, clinical lithotripsy is typically performed between 300 mJ/pulse to 2 J/pulse. These high energy levels are necessary to raise the temperature of the target calculus over the threshold breakdown temperature of its chemical composition, as opposed to the temperature needed for water vaporization.

In air, all Ho:YAG energy was deposited directly onto the surface of the dried urinary calculus, producing the greatest mass-loss among the three scenarios (Table 2). For hydrated urinary

calculus, some laser energy was required to heat and possibly vaporize surface and interstitial water. For urinary calculi submerged in water, more energy was needed to vaporize the water layer between the fiber-tip and the surface of the calculus in addition to heating interstitial water. Therefore, it is not surprising that calculus in water yielded the least amount of mass-loss. It is likely that interstitial water expansion and explosive vaporization do not contribute directly to fragmentation, but may facilitate the ejection of decomposed stone fragments (or cysteine and free sulfur gas in the case of cystine lithotripsy) as can be seen in the plume formation which begins about 50 μs after the initiation of Ho:YAG irradiation (Fig. 3).

Izatt et al. have theorized that water within bone (hydroxyapatite) is heated upon Ho:YAG irradiation [35]. As this water rapidly vaporizes, it produces momentum necessary for calcium fragment ejection. This thermal mechanism on explosive vaporization of interstitial water has been proposed for Ho:YAG lithotripsy [29]. However, it is well known that clinical long-pulse Ho:YAG laser ablation of calcified tissue occurs without significant thermal damage to surrounding tissue, i.e., thermal confinement occurs [36]. In addition, holmium lithotripsy creates sharply demarcated craters, with microscopic preservation of crystalline lamella on the crater surface, implying a regular, consistent, and stereotypical laser-calculus interaction [9]. All these observations indicate that holmium lithotripsy is governed by thermal breakdown of calculus composition through direct laser absorption, whereas interstitial water and vapor expansion merely facilitates the ejection of fragments within the volume of decomposed compounds, leaving the parent calculus or original compound intact.

Mass-loss measurement based on the initial temperature of calculus further strengthens the hypothesis of a dominant photothermal lithotripsy. COM and cystine calculi produce lower mass-loss when the calculi are ablated after removing from a –80°C freezer, compared to calculi at room temperature. The study shows that more laser energy must be deposited for the pre-cooled calculi to overcome the thermal threshold temperature for chemical breakdown.

The confirmation that long-pulse Ho:YAG lithotripsy is due to photothermal effects has important clinical implications. The finding that one thermal by-product of uric acid lithotripsy is cyanide, raises safety issues [11,37–39]. Lithotripsy of the holmium laser is most efficient in the contact mode with the delivery fiber placed perpendicular to the calculus surface for laser-calculus interaction. LISL, however, requires a small fiber-calculus separation to maximize the coupling of photoacoustical energy [16–19,24]. In addition, since shock waves propagate spherically, LISL risks collateral mucosal injury and bleeding. The holmium laser does not generate significant shock waves and its thermally-induced fragmentation is highly directional as reported in the fiber orientation experiments above. Hence, the long-pulse Ho:YAG laser is a solution to the problem of collateral tissue damage. Finally, the negligible mechanical effects should minimize the problem of stone migration during treatment.

CONCLUSION

We conclude that long-pulse Ho:YAG laser lithotripsy is primarily a photothermal mechanism. Direct irradiance of the urinary calculi by the holmium laser through a laser-induced vapor channel (the “Moses effect”) increases the temperature of the irradiated volume above a critical threshold temperature, causing the chemical breakdown of the calculus. Chemical breakdown weakens the mechanical integrity of the irradiated volume, allowing the vapor bubble and interstitial water or vapor expansion to facilitate the ejection of fragmented breakdown products.

REFERENCES

1. Yiu MK, Liu PL, Yiu TF, Chan AYT. Clinical experience with holmium:YAG laser lithotripsy of ureteral calculi. Lasers Surg Med 1996;19:103–106.
2. Razvi HA, Denstedt JD, Chun SS, Sales JL. Intracorporeal lithotripsy with the holmium:YAG laser. J Urology 1996;156:912.
3. Das A, Erhard MJ, Bagley DH. Intrarenal use of the holmium laser. Lasers Surg Med 1996;19:103–106.
4. Adams DH. Holmium:YAG laser and pulsed dye laser: a cost comparison. Lasers Surg Med 1997;21:29–31.
5. Teichman JMH, Rao RD, Rogenes VJ, Harris JM. Ureteroscopic management of ureteral calculi: electrohydraulic versus holmium:YAG lithotripsy. J Urology 1997; 158:1357–1361.
6. Teichman JMH, Glickman RD, Harris JM, Holmium:YAG percutaneous nephrolithotomy: the laser incident angle matters. J Urology 1998;159:690–694.
7. Dushinski JW and Lingeman JE. High-speed photographic evaluation of holmium laser. J Endourology 1998;12(2):177–181.
8. Teichman JMH, Vassar GJ, Bishoff JT, Bellman GC. Holmium:YAG lithotripsy yields smaller fragments than

pulsed dye, lithoclast, or electrohydraulic lithotripsy. J Urology 1998;159:18–27.
9. Vassar GJ, Teichman JMH, Glickman RD. Holmium:YAG lithotripsy efficiency varies with energy density. J Urology 1998;160: 471–476.
10. Teichman JMH, Vassar GJ, Glickman RD. Holmium: YAG lithotripsy efficiency varies with stone composition. J Urology 1998;52:392–397.
11. Teichman JMH, Vassar GJ, Glickman RD, Beserra CM, Cina SJ, Thompson IM. Holmium:YAG lithotripsy: photothermal mechanism converts uric acid calculi to cyanide. J Urology 1998;160:320–324.
12. Teichman JMH, Rogenes VD, McIver BJ, Harris JM. Holmium:YAG laser cystolithotripsy of large bladder calculi. J Urology 1997;50:44.
13. Thomas S, Pensel J, Engelhardt R, Meyer W, Hofstetter AG. The pulsed dye laser versus the Q-switched Nd:YAG laser in laser-induced shock-wave lithotripsy," Lasers Surg Med 1988;8:363–370.
14. Spindel ML, Moslem A, Bhatia KS, Jassemnejad B, Bartels KE, Powell RC, O'Hare CM, Tytle T. Comparison of holmium and flashlamp pumped dye lasers for use in lithotripsy of biliary calculi," Lasers Surg Med 1992;12: 482–489.
15. Goldey CL, Rosen DI, Hayes GB, Willscher MK, Roth RA. Development of a smart Holmium:YAG laser lithotriptor. Lasers Surg Med 1997;21:20–28.
16. Rink K, Delacretaz G, Salathe RP. Fragmentation process induced by nanosecond laser pulses. Appl Phys Lett 1992;61(22):2644–2646.
17. Rink K, Delacretaz, Salathe RP. Influence of the pulse duration on laser induced mechanical effects. SPIE 1994; 2077:181–194.
18. Rink K, Delacretaz G, Salathe RP. Fragmentation process of current laser lithotriptors. Lasers Surg Med 1995; 16:134–146.
19. Rink K, Delacretaz G, Salathe RP. Fragmentation process induced by microsecond laser pulses during lithotripsy. Appl Phys Lett 1992;61(3):258–260.
20. Jansen ED, Asshauer T, Frenz M, Motamedi M, Delacretaz G, Welch AJ. Effect of pulse duration on bubble formation and laser-induced pressure waves during holmium laser ablation. Lasers Surg Med 1996;18: 278–293.
21. Schafer SA, Durville FM, Jassemnejad B, Bartels KE, Powell RC. Mechanisms of biliary stone fragmentation using the Ho:YAG laser. IEEE Trans On Biomedical Engineering March 1994;41(3):276–283.
22. Isner JM. Blood. In Isner JM, Clarke R, editors. Cardiovascular Laser Therapy. New York: Raven Press; 1989. p 39–62.
23. Jacques SL. Laser-tissue interactions: photochemical, photothermal, and photomechanical. Surg Clin N Am 1992;72:531–558.
24. Zhong P, Tong HL, Malenbaum J, Cocks FH, Preminger GM. Transient cavitation and acoustic emission produced by different laser lithotripters. J Endourology 1998;12(4): 371–378.
25. Rieders F, Cyanides, Type B procedure. In Sunshine I, editor. Methodology for analytical toxicology. Cleveland: CRC Press; 1975. p 114–115.
26. Jansen ED, van Leeuwen TG, Motamedi M, Borst C, Welch AJ. Temperature dependency of the absorption coefficient of water for mid-infrared laser radiation. Lasers Surg Med 1994;14:258–264.
27. Welch AJ, van Gemert MJC. Optical-thermal response of laser-irradiated tissue. New York: Plenum Press; 1995. p 709–763.
28. Frenz M, Pratisto H, Konz F, Jansen ED, Welch AJ, Weber HP. Comparison of the effects of absorption coefficient and pulse duration of 2.12 μm and 2.79 μm radiation on ablation of tissue. IEEE J Quantum Electronics 1996;32(12):2025–2036.
29. Beghuin D, Delacretaz G, Schmidlin F, Rink K. Fragmentation process during Ho:YAG laser lithotripsy revealed by time-resolved imaging. SPIE 1998;3195:220–224.
30. Koechner W, Solid-state laser engineering. Springer Series in Optical Sciences, 3rd Edition. New York: Springer-Verlag; 1992. p 282.
31. Lauterborn W, Bolle H. Experimental investigations of cavitation-bubble collapse in the neighbourhood of a solid boundary. J Fluid Mech 1975;72(2):391–399.
32. Plesset MS, Chapman RB. Collapse of an initially spherical vapour cavity in the neighbourhood of a solid boundary. J Fluid Mech 1971;47(2):283–290.
33. Godwin RP, Chapyak EJ. Laser mass ablation efficiency measurements indicate bubble-driven dynamics dominates laser thrombolysis. SPIE 1998;3245:4–11.
34. Rudhart M, Hirth A. Use of an absorbent in laser lithotripsy with dye lasers: in vitro study of fragmentation efficiency and jet formation. J Urology 1994;152:1005–1008.
35. Izatt JA, Albagli D, Itzkan I, Feld M. Pulsed laser ablation of calcified tissue: physical mechanisms and fundamental parameters. SPIE 1990;1202:133–140.
36. Cervanin I. A comparison of the effects of Nd:YAG and Ho:YAG laser irradiation on dentine and enamel. Aust Dent J 1995;40:79–84.
37. Mahn WJ. Academic laboratory chemical hazards guidebook. New York: Van Nostrand Reinhold; 1991. p 187–190.
38. Ballantyne B, Mares TC. Toxicology of cyanides. Bristol: Wright and Sons; 1987.
39. Teichman JMH, Champion PC, Wollin TA, Denstedt JD. Holmium:YAG lithotripsy of uric acid calculi. J Urology 1998;160:2130–2132.
40. Budavari S, O'Neil MJ, Smith A, Heckelman PE, editors. The Merck Index. Rahway, NJ: Merck & Co.; 1989.